

Initial observations from the Lunar Orbiter Laser Altimeter (LOLA)

David E. Smith,^{1,2} Maria T. Zuber,¹ Gregory A. Neumann,² Frank G. Lemoine,² Erwan Mazarico,² Mark H. Torrence,³ Jan F. McGarry,² David D. Rowlands,² James W. Head III,⁴ Thomas H. Duxbury,⁵ Oded Aharonson,⁶ Paul G. Lucey,⁷ Mark S. Robinson,⁸ Olivier S. Barnouin,⁹ John F. Cavanaugh,¹⁰ Xiaoli Sun,² Peter Liiva,¹¹ Dan-dan Mao,¹¹ James C. Smith,¹⁰ and Arlin E. Bartels¹⁰

Received 26 April 2010; revised 8 June 2010; accepted 14 June 2010; published 18 September 2010.

[1] As of June 19, 2010, the Lunar Orbiter Laser Altimeter, an instrument on the Lunar Reconnaissance Orbiter, has collected over 2.0×10^9 measurements of elevation that collectively represent the highest resolution global model of lunar topography yet produced. These altimetric observations have been used to improve the lunar geodetic grid to ~ 10 m radial and ~ 100 m spatial accuracy with respect to the Moon's center of mass. LOLA has also provided the highest resolution global maps yet produced of slopes, roughness and the 1064-nm reflectance of the lunar surface. Regional topography of the lunar polar regions allows precise characterization of present and past illumination conditions. LOLA's initial global data sets as well as the first high-resolution digital elevation models (DEMs) of polar topography are described herein. **Citation:** Smith, D. E., et al. (2010), Initial observations from the Lunar Orbiter Laser Altimeter (LOLA), *Geophys. Res. Lett.*, 37, L18204, doi:10.1029/2010GL043751.

1. Introduction

[2] Assessment of robotic or human landing sites on a planetary surface requires precise characterization of elevations at a range of spatial scales, as well as global geolocation to enable precision targeting and correlation of data sets. The Lunar Orbiter Laser Altimeter (LOLA) [Smith *et al.*,

2010], a payload element on the Lunar Reconnaissance Orbiter (LRO) [Chin *et al.*, 2007] was designed to characterize landing sites and to provide a precise global geodetic grid on the Moon. LOLA's primary measurement is surface topography, and in addition the instrument provides ancillary measurements of surface slope, roughness and 1064-nm reflectance. This paper describes LOLA's initial global data sets, which have greater accuracy and are more complete in coverage than provided by previous altimeters and Earth-based radar.

2. The Lunar Orbiter Laser Altimeter

[3] LOLA [Smith *et al.*, 2010] is a multi-beam laser altimeter that operates at a wavelength of 1064.4 nm with a 28-Hz pulse repetition rate. A single laser beam is split by a diffractive optical element into five output beams, each of which has a $100\text{-}\mu\text{rad}$ divergence and illuminates a 5-m-diameter spot from LRO's mapping orbit, resulting in a total sampling rate of the lunar surface of 140 measurements/sec. Backscattered pulses are detected by the receiver, which images the 5-spot pattern onto separate optical fibers, each of which relays the received signal to a distinct silicon avalanche photodiode detector.

[4] LOLA's sampling strategy produces 5 parallel profiles along LRO's sub-spacecraft ground track. Profiles are 10–12-m apart with observations within each profile separated by ~ 56 m, determined by the laser pulse repetition rate and spacecraft velocity. The laser spots form a cross pattern on the lunar surface (Figure 1a), with each beam separated by an angle of $500\text{ }\mu\text{rad}$ and rotated 26° about the nadir axis with respect to the spacecraft forward velocity vector. The sampling pattern permits calculation of surface slopes along a range of azimuths.

[5] LOLA has two laser transmitters with pulse energies of 2.5 and 2.7 mJ, respectively. The lasers are operated one at a time, alternated on an approximately monthly basis in order to monitor instrument performance. Neither laser has shown a decrease in output energy since initial turn-on in July 2009. A life test of a LOLA engineering model laser in vacuum at NASA Goddard Space Flight Center as of April 6, 2010 had accumulated 1.20×10^9 pulses without any apparent degradation in performance (G. B. Shaw, personal communication, 2010).

[6] As of June 19, 2010 LOLA had acquired 2.0×10^9 altimeter measurements of lunar topography on ~ 800 mil-

¹Department of Earth, Atmospheric and Planetary Sciences, Massachusetts Institute of Technology, Cambridge, Massachusetts, USA.

²Solar System Exploration Division, NASA Goddard Space Flight Center, Greenbelt, Maryland, USA.

³SGT, Inc., Greenbelt, Maryland, USA.

⁴Department of Geological Sciences, Brown University, Providence, Rhode Island, USA.

⁵George Mason University, Fairfax, Virginia, USA.

⁶Division of Geological and Planetary Sciences, California Institute of Technology, Pasadena, California, USA.

⁷Hawaii Institute of Geophysics and Planetology, University of Hawaii, Honolulu, Hawaii, USA.

⁸School of Earth and Space Exploration, Arizona State University, Tempe, Arizona, USA.

⁹Space Department, Johns Hopkins University Applied Physics Laboratory, Laurel, Maryland, USA.

¹⁰Advanced Engineering and Technology Directorate, NASA Goddard Space Flight Center, Greenbelt, Maryland, USA.

¹¹Sigma Space Corporation, Lanham, Maryland, USA.

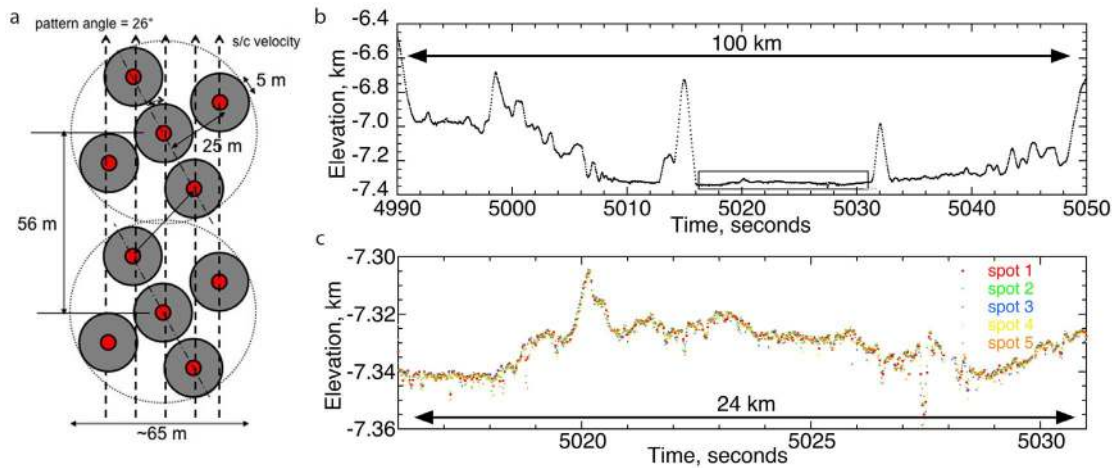


Figure 1. (a) LOLA 5-spot pattern on the lunar surface. The red area is the area illuminated by the laser and is 5 m from 50 km altitude. The gray area is the field of view of the detector; (b) LOLA single track across the floor of the Antoniadi crater (188°E, 70°S) (two inner peaks are the peak ring); and (c) a close-up highlighting the 5 laser spots within the region within the box inside the peak ring. The scatter of points along the profile is a measure of the variance in elevation within the 65-m-wide along-track sampling area.

lion pulses, increasing at rate of 190 million measurements/month.

3. Mission Phases and Instrument Operation

3.1. Commissioning Phase

[7] After insertion into lunar orbit, LRO transitioned to a 30 km × 216 km polar orbit, with periapsis near the south pole. During this spacecraft-commissioning phase, the performance of the spacecraft and the instruments was validated and instrument calibrations were performed. LOLA was turned on for an initial check on July 3, 2009 for two days and both lasers were operated. The instrument initiated continuous operation on July 13, 2009, extending through the end of commissioning in mid-September 2009. During commissioning, LOLA ranged successfully to the lunar surface from an altitude of ~190 km, roughly a factor a two larger than the design specification [Smith et al., 2010]. The instrument also acquired a significant quantity of valuable altimetry, slope and roughness data over the southern hemisphere where the spacecraft altitude was lower. Also during the commissioning phase the bore sight alignment of the LOLA receiver and the LRO spacecraft was measured by scanning LOLA toward a satellite laser ranging station at the Goddard Geophysical and Astronomical Observatory, transmitting and detecting laser pulses to and from the ground station and LOLA.

3.2. LOLA "Anomaly"

[8] When LOLA is over the sunlit side of the Moon all 5 receiver channels receive returns from the surface continuously and the instrument acquires data at its full rate of 140 measurements/second. Over the dark side of the Moon only 2 of the 5 receiver channels acquire significant amounts of data. Signal loss initiates as the LRO spacecraft crosses the terminator over the lunar poles. Ground testing with the LOLA engineering unit has shown that this effect is likely caused by a contraction of the spacecraft thermal blanket attached to the LOLA transmitter optics. When LRO flies

over the colder parts of the Moon the blanket pulls the transmitter beam out of alignment with the receiver. The overall LOLA data acquisition rate is between 80 and 90 valid measurements/second.

3.3. Mapping Phase

[9] The LRO spacecraft entered its mapping phase, a near-circular polar orbit at a mean altitude of 50 km, in mid-September 2009. The average separation of altimetry measurements along track for all 5 beams is ~18 m and the across track separation, which decreases with increasing number of orbits of the Moon, is currently ~1.8 km.

4. Measurements

4.1. Topography

[10] LOLA operates by measuring the two-way time of flight of each laser pulse. The time-of-flight is measured by timing the pulse leading and trailing edge threshold crossings using a set of time-to-digital-converters which provides a single-shot timing precision of 0.7 nsec over flat surfaces at nominal received signal level. The timing resolution of the LOLA receiver translates to a best-case single pulse range precision of ~9 cm. Measurement precision degrades due to surface roughness and off-nadir pointing of the LRO spacecraft. The precision of individual altimeter measurements collected so far is ~12 cm on flat (maria) surfaces. By combining the one-way range to ground points with the reconstructed orbit of the spacecraft, the radius of the Moon is calculated. Topography is determined by subtracting a sphere of 1737.4 km from each radius measurement.

4.2. Slopes

[11] Elevations provide measurements of slope over a range of baselines. Sets of 3 points in order of increasing distance along track provide a slope magnitude and azimuth for the enclosed triangle at 25–50 m baselines, spanning multiple shots if appropriate. A least-squares planar fit to sets of 4 to 10 spots provides differential slope measure-

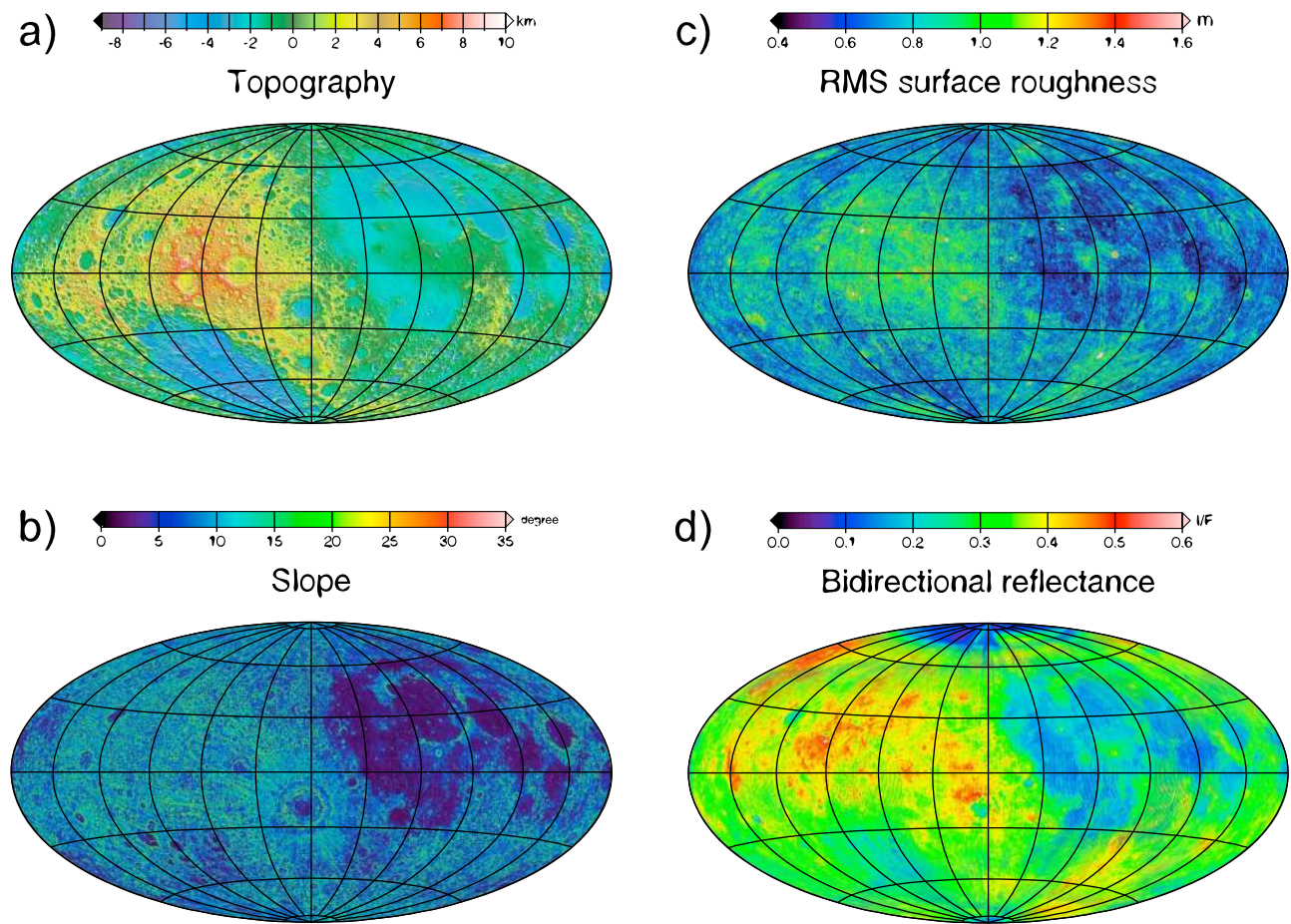


Figure 2. Hammer equal-area projections of LOLA global data sets: (a) topography, (b) surface slope over 56-m baselines, (c) surface roughness within 5-m laser footprints, and (d) six-month averages of 1064-nm bidirectional reflectance for Spot 5. In Figure 2d, I/F is the ratio of the reflected flux from the surface and the incident flux from LOLA. The coordinates of the projection have 270°E longitude in the center with 90°E on the extreme right and extreme left. The lunar nearside is on the right and the lunar farside on the left. Latitude lines are 30° apart.

ments [Kreslavsky and Head, 2000] over a two-shot (56-m) baseline, as well as topographic variance, which are relevant to landing site characterization.

4.3. Surface Roughness

[12] Spreading in time of backscattered pulses provides a measure of the root mean square (rms) roughness of the surface at the scale of the laser footprint. In LRO's mapping orbit, the preponderance of laser energy (full width at half maximum amplitude) falls within a 2.5-m-diameter circular spot that reflects on average 50% of the incident laser photons. Scattering of returns from heights varying by 30 cm (rms) extends the backscattered pulse width from that reflected from level ground. LOLA monitors the pulse width at the signal threshold crossing of the backscattered pulse, and this parameter can also be used to infer the received pulse shape. The analysis approach makes use of the area under the pulse waveform as well as threshold setting and accounts for observation errors; surface roughness as small as 1 m can be resolved [Neumann *et al.*, 2003]. The relationship between LOLA's measured pulse width as a function of the threshold value for Laser 1 and 2 was measured prior to launch for calibration purposes.

4.4. Surface Reflectivity

[13] LOLA was designed to measure pulse energy with the primary aim of being able to detect surface ice at small areal density. The ratio of returned to transmitted pulse energy represents a measure of surface reflectance at the laser wavelength. Energies of transmitted and backscattered laser pulses are measured by integrating the area under the pulses. The surface reflectance is also required for corrections to other measurements of interest to LOLA's performance such as pulse width and time walk. While the instrument does not have a self-calibration source in flight, the reflectance measurement is calibrated in a relative sense with respect to pre-launch testing.

5. Orbit Determination and Geolocation

[14] The LRO spacecraft is tracked using S Band Doppler and range data by the Universal Space Network, Deep Space Network and White Sands Missile Range. LRO also has a high-precision laser tracking system that employs stations on Earth that make one-way laser ranging measurements to a small optical receiver on the LRO high gain antenna, that detects the photons from ground stations and transmits them

Table 1. Preliminary Lunar Shape Parameters^a

Parameter	Value
Mean radius	1737153 ± 10
Center of figure, <i>x</i>	−1777 ± 3
Center of figure, <i>y</i>	−732 ± 3
Center of figure, <i>z</i>	240 ± 3
Polar flattening	1494 ± 10
Radius, X-axis	Mean radius + 45 ± 10
Radius, Y-axis	Mean radius + 247 ± 10
Shape $C_{2,0}$	−668.0 ^b
Shape $C_{2,2}$	108.7 ^b
Shape $S_{2,2}$	383.2 ^b

^aError estimates include approximate uncertainties for the orbital position of LRO. Values in meters.

^bNormalized.

to LOLA's central detector via an optical fiber bundle [Zuber *et al.*, 2010]. Participating Earth laser stations operate either synchronously at the LOLA rate of 28 Hz to ensure returns within the 8-ms Earth-ranging window, or asynchronously at another rate at a reduced detection rate at LOLA. Laser ranging data are returned to Earth via the LOLA data stream and are incorporated into orbit determination analyses. These observations, which are accurate to a few cm averaged over 5 seconds, improve the position of LRO and will ultimately enable improvement of the lunar gravity model. Earth-based laser ranging is also used to monitor the stability of LRO's primary oscillator, over hours to months time scale. The laser ranging capability helps LRO to maintain <1 msec timing accuracy with respect to UTC for LOLA and the other LRO instruments.

[15] Elevations herein were determined using LRO navigation orbits. These orbits dictate that the current accuracy of individual LOLA ground points is ~10 m in the radial direction and ~50 and ~100 m across track and along track, respectively. Orbit reconstructions using Lunar Prospector gravity models such as LP150Q [Konopliv *et al.*, 2001] and GLGM-3 [Mazarico *et al.*, 2010], or Kaguya-based models such as SGM100H [Matsumoto *et al.*, 2010] are of comparable quality.

6. LOLA Profiles

[16] The lowest point on the Moon lies on the floor of the farside Antoniadi crater. At ~143 km diameter, Antoniadi is one of the few lunar craters that exhibits both a central peak and a surrounding peak ring, and thus provides insight into the transition from complex craters to ringed basins [Wilhelms, 1987]. Antoniadi's low elevation, explainable in part by its location on the floor of the South Pole-Aitken basin, combined with its geometric structure and the occurrence of very young maria on its floor [Haruyama *et al.*, 2009], make this crater of prime interest.

[17] An example of a LOLA 5-profile pass crossing Antoniadi is shown in Figure 1b. Nearly 100% of output pulses are received along the track that included along-track slopes up to 15°. The location and detailed character of the peak ring and its relationship to rim crest collapse and terracing are readily documented and the embayment relationships of the younger maria and impact melt on the crater floor are clear. Figure 1c shows a close-up of the central crater floor within the peak ring as denoted in Figure 1b and the 5 beams reveal the complex structure of the floor; with 10-cm preci-

sion the dispersion of points is predominantly a measure of rms surface variance across the profiles. A low broad rise is revealed in the detailed LOLA data suggesting a combination of topography from individual lava flows and broad deformation of the inner crater floor. Furthermore, the dispersion of points permits the detailed comparison of this very young mare deposit [Haruyama *et al.*, 2009] with older lunar maria deposits to document the evolution of mare regolith at human-robotic exploration scales. The profiles across Antoniadi exemplify the utility of LOLA's high spatial and radial resolution for understanding the contributions of impact cratering, tectonism and volcanism in shaping the lunar surface.

7. Global Data Sets

7.1. Topography

[18] LOLA altimetry data have been used to develop a global grid of topography and Figure 2a shows the global model plotted at a resolution of 1/16° (2 km). The highest elevation is 10.7834 km at 201.378°E, 5.401°N, and the lowest elevation of −9.117 km lies at 187.5074°E, 70.360°S within the Antoniadi crater (cf. Figure 1b). The along-track spatial resolution of the full global data set is about 20 m and the cross-track resolution is ~0.07°, corresponding to ~1.8 km at the equator and 160 m at 85° lat.

[19] A spherical harmonic expansion of the gridded data to degree and order 720 (spatial block size 7.5 km) yields fundamental parameters of the lunar shape (Table 1). The degree-2 shape is dominated by the flattening ($C_{2,0}$) and the nearside southern highland/farside highland relief. The nearside northern maria and farside equatorial highlands give rise to a large equatorial ellipticity ($C_{2,2}$) in the global shape, as well as to a significant $C_{4,0}$ term. Since terranes are to first order compensated by crustal thickness and density variations [Neumann *et al.*, 1996], the $C_{2,0}$ term does not result in a correspondingly large gravitational potential $C_{2,1}$, that would tilt the Moon. A manifestation of the large $C_{4,0}$ term is that the Moon's mean equatorial radius and polar radii are both greater than the global mean radius. Consequently, in contrast to past practice [Yoder, 1995], a triaxial ellipsoid is not a particularly good description of the Moon's global shape.

7.2. Slopes

[20] Figure 2b shows a map of bidirectional slope magnitudes with spatial resolution of ~50 m. Data was binned at 16 pixels/degree, and the median value reported. As for Mars [Aharonson *et al.*, 2001; Kreslavsky and Head, 2000], different geologic units have distinct slope and roughness properties. A region selected as representative of maria topography (−75 to 30 E, 30 to 60 N) exhibits a median slope of ~3.8°, while a region representative of highlands (180 to 240 E, 5 to 60 N) has a steeper median slope of ~9.8°. Fully 95% of slopes are shallower than ~17.5° in the maria, and than ~25.2° in rougher highlands. Analysis is ongoing to classify and interpret geologic units according to statistical topographic properties [Rosenburg *et al.*, 2010].

7.3. Surface Roughness

[21] Surface roughness from pulse spreading at 5-m spatial scale is shown in Figure 2c. Pulse widths are visibly widened on crater rims, basin rings, central peaks, the aprons of some impact structures and South Pole-Aitken massifs,

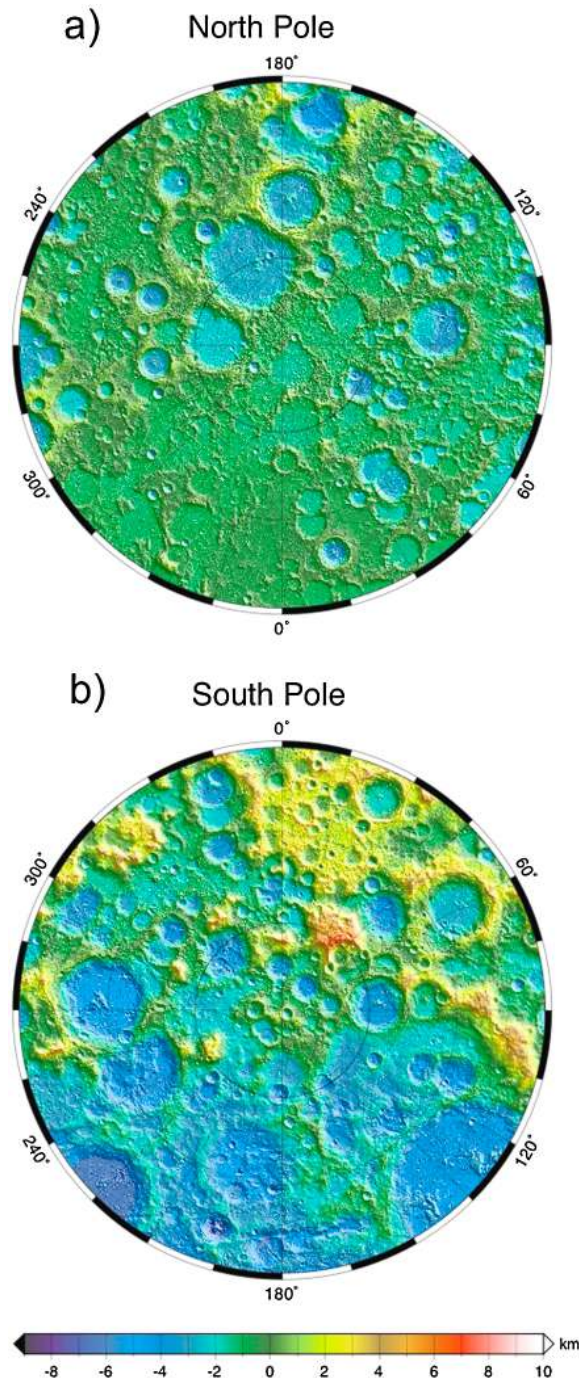


Figure 3. Polar stereographic projections of topography at the lunar (a) north pole and (b) south pole to 75° latitude.

among other structures. Further calibration of pulse widths against threshold, energy and instrument parameters will provide a globally consistent quantitative measure of lunar roughness at the scale of a few meters.

7.4. The 1064-nm Surface Reflectivity

[22] Measurement of reflectance from LOLA is challenging due to signal loss at terminator crossings as discussed above. Consequently the primary objective of the reflectance measurement, the search for surficial polar ice, is the subject of on-going analysis. However, away from ter-

minator crossings LOLA's pulse energy measurement provides a unique new view of the reflectance of the Moon. In Figure 2d the brighter anorthositic highlands and darker basaltic maria are apparent as they are in other near-IR spectral maps. But unlike all previous imaging measurements that must contend with highly variable lighting and lunar bidirectional reflectance variations from terrain to terrain, LOLA observes the lunar surface at zero phase. This highly uniform illumination allows the reflectance of different lunar terrains to be compared very precisely with none of the potential systematic errors due to uncertainty in lunar photometric properties that plague passive imaging sensors. This measurement is a critical check on surface properties derived from other sensors that include latitude-dependent normalizations, especially in the polar regions, which cannot be characterized photometrically by passive imaging.

8. Polar Topography

[23] The LRO mission is tasked with detailed characterization of the lunar polar regions to assess the existence of volatiles. Earlier studies addressed illumination of the lunar south pole from Clementine imagery [Shoemaker *et al.*, 1994], and the possible existence of areas of near-continuous shadowing and illumination. But because the Clementine laser altimeter did not sample the poles, initial estimates of the topographic variance that resulted in visual illumination patterns were based on extrapolation of the topographic power spectrum of equatorial and mid-latitude regions [Zuber and Smith, 1997]. Topographic maps of the north and south poles were produced by Kaguya and Chang'E laser altimeters [Araki *et al.*, 2009; Huang *et al.*, 2009]. Recently, the lighting conditions at the south pole have been extensively studied with the Kaguya altimeter data [Noda *et al.*, 2008], and by the Earth-based Goldstone Solar System Radar [Bryant, 2010], though the latter is plagued by large gaps in spatial coverage due to poor geometric viewing conditions.

[24] LOLA data provide the highest-resolution, uniformly consistent spatial topographic characterization of lunar polar regions that permits a highly accurate assessment of present and past illumination conditions (E. Mazarico *et al.*, Illumination conditions of the lunar polar regions using LOLA topography, submitted to *Icarus*, 2010). Figure 3 shows DEMs of both poles. The north polar map contains 48 million elevations while the south polar map contains 92 million elevations. The south pole coverage is denser than in the north because of the favorable southern summer season in the first part of the LRO mission, and extra data collected during commissioning phase. The polar maps are shown at a resolution of 240 m, but the effective density is higher poleward of 85° due to orbit track convergence. A wide variety of crater depths and degradation states are observed; some crater walls display slopes in excess of 35°.

9. Summary

[25] LOLA has provided the highest-resolution global models of topography, slope and surface roughness, and a near global model of 1064-nm reflectance. Data collection continues through LRO's mapping cycle. LOLA continues to operate to improve, in particular, the cross-track resolution of global data sets and DEMs.

[26] **Acknowledgments.** The LOLA investigation is supported by the LRO Project under contract from the NASA Exploration Systems Mission Directorate. We thank Patrick McGovern and Hiroshi Araki for helpful reviews. LOLA data and products are downloadable from <http://pds-geosciences.wustl.edu/missions/lro/lola.htm>.

References

- Aharonson, O., M. T. Zuber, and D. H. Rothman (2001), Statistics of Mars' topography from the Mars Orbiter Laser Altimeter (MOLA): Slopes, correlations and physical models, *J. Geophys. Res.*, **106**, 23,723–23,735.
- Araki, H., et al. (2009), Lunar global shape and polar topography derived from KAGUYA-LALT laser altimetry, *Science*, **323**, 897–900, doi:10.1126/science.1164146.
- Bryant, S. (2010), Lunar pole illumination and communications statistics computed from GSSR elevation data, paper presented at Space Ops 2010, Am. Inst. of Aeronaut. and Astronaut., Huntsville, Ala.
- Chin, G., et al. (2007), Lunar Reconnaissance Orbiter overview: The instrument suite and mission, *Space Sci. Rev.*, **129**, 391–419, doi:10.1007/s11214-007-9153-y.
- Haruyama, J., et al. (2009), Long-lived volcanism on the lunar farside revealed by SELENE terrain camera, *Science*, **323**, 905–908, doi:10.1126/science.1163382.
- Huang, Q., et al. (2009), New features of the Moon revealed and identified by CLTM-s01, *Sci. Chin. Ser. G*, **52**, 1815–1823.
- Konopliv, A. S., S. W. Asmar, E. Carranza, W. L. Sjogren, and D.-N. Yuan (2001), Recent gravity models as a result of the Lunar Prospector mission, *Icarus*, **150**, 1–18, doi:10.1006/icar.2000.6573.
- Kreslavsky, M. A., and J. W. I. Head III (2000), Kilometer-scale roughness of Mars: Results from MOLA data analysis, *J. Geophys. Res.*, **105**, 26,695–26,711.
- Matsumoto, K., et al. (2010), An improved lunar gravity field model from SELENE and historical tracking data: revealing the farside gravity features, *J. Geophys. Res.*, **115**, E06007, doi:10.1029/2009JE003499.
- Mazarico, E., et al. (2010), GLGM-3, a degree 150 lunar gravity model From the historical tracking data of NASA moon orbiters, *J. Geophys. Res.*, **115**, E05001, doi:10.1029/2009JE003472.
- Neumann, G. A., M. T. Zuber, D. E. Smith, and F. G. Lemoine (1996), The lunar crust: Global signature and structure of major basins, *J. Geophys. Res.*, **101**, 16,841–16,863, doi:10.1029/96JE01246.
- Neumann, G. A., J. B. Abshire, O. Aharonson, J. B. Garvin, X. Sun, and M. T. Zuber (2003), Mars Orbiter Laser Altimeter measurements of pulse width and footprint-scale roughness, *Geophys. Res. Lett.*, **30**(11), 1561, doi:10.1029/2003GL017048.
- Noda, H., H. Araki, S. Goossens, Y. Ishihara, K. Matsumoto, S. Tazawa, N. Kawano, and S. Sasaki (2008), Illumination conditions at the lunar polar regions by KAGUYA (SELENE) laser altimeter, *Geophys. Res. Lett.*, **35**, L24203, doi:10.1029/2008GL035692.
- Rosenburg, M., et al. (2010), Lunar surface roughness and slope statistics from LOLA, *Lunar Planet. Sci. Conf., XIL*, Abstract 2502.
- Shoemaker, E. M., et al. (1994), The south pole region of the Moon as seen by Clementine, *Science*, **266**, 1851–1854, doi:10.1126/science.266.5192.1851.
- Smith, D. E., et al. (2010), The Lunar Orbiter Laser Altimeter investigation on the Lunar Reconnaissance Orbiter mission, *Space Sci. Rev.*, **150**, 209–241, doi:10.1007/s11214-009-9512-y.
- Wilhelms, D. E. (1987), *The Geologic History of the Moon*, 302 pp., U.S. Gov. Print. Off., Washington, D. C.
- Yoder, C. F. (1995), Astrometric and geodetic properties of Earth and the Solar System, in *Global Earth Physics, A Handbook of Physical Constants*, *AGU Ref. Shelf*, vol. 1, edited by T. J. Ahrens, pp. 1–32, AGU, Washington, D. C.
- Zuber, M. T., and D. E. Smith (1997), Topography of the lunar south polar region: Implications for the size and distribution of permanently shaded areas, *Geophys. Res. Lett.*, **24**, 2183–2186, doi:10.1029/97GL02111.
- Zuber, M. T., et al. (2010), The Lunar Reconnaissance Orbiter laser ranging investigation, *Space Sci. Rev.*, **150**, 63–80, doi:10.1007/s11214-009-9511-z.
- O. Aharonson, Division of Geological and Planetary Sciences, California Institute of Technology, Pasadena, CA 91125, USA.
- O. S. Barnouin, Space Department, Johns Hopkins University Applied Physics Laboratory, Laurel, MD 20723, USA.
- A. E. Bartels, J. F. Cavanaugh, and J. C. Smith, Advanced Engineering and Technology Directorate, NASA Goddard Space Flight Center, Greenbelt, MD 20771, USA.
- T. H. Duxbury, Department of Physics and Astronomy, George Mason University, Fairfax, VA 22030, USA.
- J. W. Head III, Department of Geological Sciences, Brown University, Providence, RI 02912, USA.
- F. G. Lemoine, E. Mazarico, J. F. McGarry, G. A. Neumann, D. D. Rowlands, and X. Sun, Solar System Exploration Division, NASA Goddard Space Flight Center, Greenbelt, MD 208771, USA.
- P. Liiva and D. Mao, Sigma Space Corporation, Lanham, MD 20706, USA.
- P. G. Lucey, Hawaii Institute of Geophysics and Planetology, University of Hawaii, Honolulu, HI 96822, USA.
- M. S. Robinson, School of Earth and Space Exploration, Arizona State University, Tempe, AZ 85287, USA.
- D. E. Smith and M. T. Zuber, Department of Earth, Atmospheric and Planetary Sciences, Massachusetts Institute of Technology, Cambridge, MA 02139, USA. (zuber@mit.edu)
- M. H. Torrence, SGT, Inc., 7701 Greenbelt Rd., Greenbelt, MD 20770, USA.